http://doi.org/10.35784/iapgos.2855

ELLIPSOMETRY BASED SPECTROSCOPIC COMPLEX FOR RAPID ASSESSMENT OF THE $Bi_2Te_{3-x}Se_x$ THIN FILMS COMPOSITION

Vladimir Kovalev[1], Saygid Uvaysov[2], Marcin Bogucki[3]
[1]MOCVD Semiconductor Growth Laboratory, Kotelnikov Institute of Radio-Engineering and Electronics of RAS, Fryazino, Russia, [2]MIREA – Russian Technological University, Moscow, Russia, [3]Lublin University of Technology, Faculty of Mechanical Engineering, Lublin, Poland

Abstract. *A comparative analysis of the current state and development of spectral ellipsometry (SE) is carried out, the main limitations typical of popular configurations of measuring devices are determined. An original technical solution is proposed that allows one to create a two-source SE that implements the ellipsometry method with switching orthogonal polarization states. The measuring setup provides high precision of measurements of ellipsometric parameters Ψ and Δ in the spectral range of 270–2200 nm and the speed determined by the characteristics of pulsed sources with a simple ellipsometer design. As objects for experimental researches, confirming the efficiency and high precision qualities of the fabricated SE, we used a GaAs/ZnS-quarter-wave device for a CO_2 laser and SiO_2 on Si calibration plates. The optical properties of $Bi_2Te_{3-x}Se_x$ films were investigated in the range of 270–1000 nm using a multi-angle SE. It was shown that the optical properties of $Bi_2Te_{3-x}Se_x$ films monotonically change depending on the ratio of selenium and tellurium.*

Keywords: thin films, optical properties, spectroscopy, Fourier transform, ellipsometry and polarimetry, optics on surfaces, instrumentation, measurements and metrology

ELIPSOMETRYCZNY SYSTEM SPEKTROSKOPOWY DO SZYBKIEJ OCENY SKŁADU CIENKICH WARSTW $Bi_2Te_{3-X}Se_X$

Streszczenie. *W artykule najpierw dokonano analizy porównawczej obecnego stanu rozwoju elipsometrii spektroskopowej oraz określono główne ograniczenia typowe dla popularnych konfiguracji urządzeń pomiarowych. Zaproponowano oryginalne rozwiązanie techniczne pozwalające na stworzenie dwuźródłowego elipsometu spektroskopowego z przełączaniem ortogonalnych stanów polaryzacji. Układ pomiarowy zapewnia wysoką precyzję pomiarów parametrów elipsometrycznych Ψ i Δ w zakresie spektralnym 270–2200 nm i prędkości wyznaczonej przez charakterystyki źródeł impulsowych przy prostej konstrukcji elipsometru. Jako obiekty do badań eksperymentalnych potwierdzających wydajność i wysoką precyzję proponowanego elipsometu spektroskopowego, wykorzystano ćwierćfalowy przyrząd GaAs/ZnS dla lasera CO_2 oraz płytki kalibracyjne SiO_2 na krzemie. Właściwości optyczne warstw $Bi_2Te_{3-x}Se_x$ zbadano w zakresie 270–1000 nm przy użyciu wielokątowego elipsometu spektroskopowego. Wykazano, że właściwości optyczne cienkich warstw $Bi_2Te_{3-x}Se_x$ zmieniają się monotonicznie w zależności od stosunku zawartości selenu i telluru.*

Słowa kluczowe: cienkie warstwy, właściwości optyczne, spektroskopia, transformata Fouriera, elipsometria i polarymetria, optyka cienkowarstwowa, oprzyrządowanie, pomiary i metrologia

Introduction

Over the past years, the method of spectral ellipsometry (SE) has become well studied [10]. This method of analytical measurements is beginning to play an increasing role in various industrial and scientific industries [18]. SE finds application in such applications as the determination of the optical characteristics of thin films [22], in-situ monitoring of semiconductor thin films and their functionality [2, 7], as well as currently topical surface probing in biochemical reactions [16, 17]. In addition, ellipsometry provides exceptional measurement sensitivity, which makes it possible to use it for monitoring the epitaxial growth of thin films with submonolayer resolution [14, 20].

SE measures the changes in the polarization of light that occur when reflected from the surface of a sample depending on the wavelength of light to determine material properties such as complex dielectric function, carrier structure, crystalline nature, and thin film thickness [21]. This change can be described by the ellipsometric angles Ψ and Δ, which represent the amplitude and phase of the complex reflectance.

$$\rho = \frac{r_p}{r_s} = tg\Psi \, exp(i\Delta), \tag{1}$$

where the parameters r_p and r_s are the complex reflection coefficients for parallel and perpendicular polarizations of light, respectively. In a conventional SE the ellipsometric parameters are obtained from measurements of the optical intensity resulting from modulation of the polarization state of light interacting with the sample material.

The spectral regions of the SE cover the ultraviolet (UV), visible and infrared (IR) spectral ranges. Relevant problems in the development of new SE are expansion in the IR spectral range, increasing the accuracy and speed of measuring ellipsometric parameters, simplifying the design of the measuring path with the exclusion of moving polarizing optical elements [3]. Well-known firms solve complex problems of development and manufacture of such SE for various purposes with extremely high technical characteristics [9]. At the same time, the most widely represented on the commercial market are SE based on the use of rotating polarizing elements [4–6] and ellipsometers with phase modulation [1, 8, 19]. For these configurations of spectral ellipsometers, typical examples with distinctive features can be given.

The ellipsometer (RC2, JAWoollam Co. Inc.) with a double rotary compensator and Muller Matrix (MM) measurement [5] is the first commercial MM ellipsometer that uses the latest InGaAs thermoelectric cooled strained array to record hundreds of wavelengths in the IR range up to 2500 nm. The Sentech SE uses a method of discrete change in the azimuths of the polarizing elements. However, this mechanical modulation of polarization limits the stability in the presence of vibrations and the stability of such SE. An ellipsometer (UVISEL Plus, HORIBA) based on phase modulation technology covers a spectral range of 190–2100 nm. Very fast acquisition rate of up to 50 ms/point, ideal for real-time kinetic studies. But the wavelength range and temperature dependence of polarization modulation provided by such devices is a limiting factor. In addition, the fast polarization modulation produced by PEM or EOM (usually from several tens of kilohertz to several tens of megahertz) makes it difficult to use a multichannel spectrometer equipped with a CCD or CMOS camera.

To overcome these limitations, we propose a SE with switching orthogonal polarization states (SOPS), since it has a number of advantages and does not contain moving polarization elements. In publications [12, 13, 15] technical indicators of spectral ellipsometers with switching orthogonal polarization states for various purposes are given.

The use of a set of eight light-emitting diodes (LEDs) in a multichannel SE with binary modulation of the polarization state [12] made it possible to develop a simple ellipsometer with a full wavelength range of 350–810 nm and high characteristics. The obtained reproducibility and stability of measurements of ellipsometric parameters Ψ and Δ are 0.01 and 0.03°, respectively. An LED ellipsometer with an extended wavelength range of 260–1000 nm is described in [13]. The precision of measurements and the stability of the ellipsometric parameters Ψ and Δ for silicon with its own dioxide at the maximum

wavelengths of LED radiation are not worse than 0.001 and 0.01°, respectively. At peak wavelengths corresponding to LEDs 365, 375, 390, 405, 420, and 465 nm, the precision of Ψ and Δ measurements of metal films is 0.0003 and 0.001°, respectively. The use of an original built-in monochromator provides a spectral resolution of 4 nm. LED magneto-optical SEs with SOPS [15] are the implementation of the deepest azimuthal modulation, the use of a two-channel detector, the use of a set of LEDs providing a high signal/noise ratio, and the absence of moving polarizing elements. These features significantly increased the accuracy of measuring the ellipsometric parameters Ψ and Δ of ferromagnetic materials and their changes (δΨ and δΔ) in a magnetic field. The results of measurements and calculations [11] are presented, confirming the possibility of creating stable reflective compensators for the spectral range of 200–2200 nm.

However, the use of miniature monochromators and optical shutters in the measuring paths of the above ellipsometers significantly limits their technical characteristics. The availability of commercially available automatic spectral complexes with a set of diffraction gratings for a wide spectral range (from 200 to 25000 nm) makes it possible to develop and create on their basis highly sensitive spectral ellipsometers with switching of orthogonal polarization states. This provides a high adjustable spectral resolution and a low level of scattered radiation.

This paper demonstrates the efficiency of using dual radiation sources and Glan–Thompson (GT) prisms with separation and convergence of orthogonally polarized beams, which made it possible to exclude a rather complex and intensity-weakening switch of orthogonal polarization states in the SE device. The peculiarity of the used prisms is the absence of changes in the geometry of the beams with the radiation wavelength, which makes it possible to use photodetectors with a small active area and high sensitivity. This implementation of SE measurements based on a slit monochromator opens up new ways and possibilities for future studies in the near IR spectral range. We used multi-angle spectroscopic ellipsometry (SE) to study the optical properties in the spectral range 260–1000 nm of $Bi_2Te_{3-x}Se_x$ films grown by the MOVPE method on sapphire substrates.

1. Material and methods

1.1. Experimental setup

The configuration of the developed spectral ellipsometer is shown in figure 1.

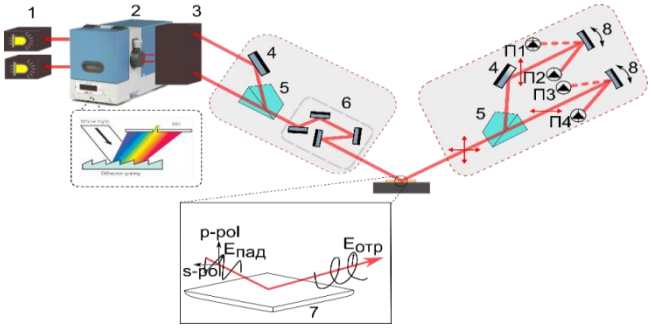

Fig. 1. TSSE optical configuration: 1 – broadband light source; 2 – monochromator; 3 – mirror system; 4 – silicon mirror; 5 – Glan-Thompson beamsplitting prism; 6 – reflective compensator; 7 – sample; 8 – rotary mirror; P1, P3 – InGaAs photodiodes; P2, P4 – silicon photodiodes

In the block of the radiation source, the halogen lamp 1 illuminates the entrance slit of the grating monochromator 2 (MDR-41, "OKB SPECTR" LLC). At the exit slit of the monochromator, there are two diaphragms 1 mm high and adjustable in width, separated by the slit height. A system of four flat and two spherical mirrors 3 (F = 65 mm) forms collimated radiation beams directed to two inputs of the GT 5 prism (calcite GBC08, Bluebean Optical Tech Ltd) with convergence of incident beams. Sequential interruption of the radiation beams from the diaphragms makes it possible to obtain collimated radiation beams with orthogonal azimuths of linear polarization P1 and P1 + 90° (P1 = 30°) at the output of the GT prism. Polarized radiation beams passing through a reflective compensator of four aluminum mirrors 6 successively fall on the sample 7 under study at an angle θ = 70°. The radiation beams reflected from the sample are divided by the second prism GT 5 into beams with orthogonal polarization azimuths A1 and A1 + 90° (A1 = 10°), which are focused by rotating mirrors 8 onto two pairs of photodetectors: P1, P3 – photodiodes InGaAs and P2, P4 – silicon photodiodes. The desired spectral dependences of the ellipsometric parameters Ψ and Δ are determined from the measured signal ratios on the photodetectors.

The method we propose can also be implemented on spectroscopic ellipsometers. In this case, the key issue is that the phase retardation of the compensator is wavelength dependent. Therefore, the optical implementation of the optimal measurement matrix must be adapted to the wavelength. On the other hand, we can also use achromatic compensators, which can provide almost the same phase delay over a wide spectral range, to implement our method for spectroscopic ellipsometers.

Compared to existing commercial ellipsometers, which use continuously rotating motors and spread the total integration time over a large number of data points, the distinct advantage of the proposed method is that it requires only four optimal intensity measurements, and the entire available integration time can be allocated to four points, which further reduces the effect of noise.

In this case, the most natural is configuration of a spectral ellipsometer with switching polarization P and P + 90° in the PSG unit using an original modulator of polarization states that does not have moving polarization elements. In this case, for the implemenatation of two more polarization states A and A + 90° in the PSA unit, a similar modulator of polarization states or a birefringent prism can be used, dividing the optical beam along the front into two orthogonal components.

Based on the proposed model of static ellipsometry with a limited number of degrees of polarization of the optical beam in the measuring path, it is possible to design a spectral ellipsometer with SOPS, which is devoid of the fundamental limitations described in the first chapter of the research, inherent in commercially available ellipsometers with rotating polarizing elements and photoelastic modulators.

Based on this scheme, we will write down an expression for the radiation intensity reaching the photodetector:

$$I_n = I_0(\sin^2 A_n \sin^2 P_n + \cos^2 A_n \cos^2 P_n \tan^2 \Psi + \\ + \frac{1}{2}\sin 2A_n \sin 2 P_n \cos \Delta \tan \Psi) \quad (2)$$

here P_n and A_n are the azimuths of the polarizer and analyzer; I_0 is an independent coefficient obtained during calibration.

Writing equation (2) for the case of four orthogonal azimuths of polarizing devices, we get:

$$I_1 = h_a\, I_0(\sin^2 A \sin^2 P + \cos^2 A \cos^2 P \tan^2 \Psi + \\ + \frac{1}{2}\sin 2A \sin 2\mathrm{P} \cos \Delta \tan \Psi)$$
$$I_2 = I_0(\cos^2 A \sin^2 P + \sin^2 A \cos^2 P \tan^2 \Psi + \\ - \frac{1}{2}\sin 2A \sin 2\mathrm{P} \cos \Delta \tan \Psi)$$
$$I_3 = h_a\, I_0(\sin^2 A \cos^2 P + \cos^2 A \sin^2 P \tan^2 \Psi + \\ - \frac{1}{2}\sin 2A \sin 2\mathrm{P} \cos \Delta \tan \Psi)$$
$$I_4 = I_0(\sin^2 A \cos^2 P + \sin^2 A \sin^2 P \tan^2 \Psi + \\ + \frac{1}{2}\sin 2A \sin 2\mathrm{P} \cos \Delta \tan \Psi) \quad (3)$$

where h_a is the coefficient describing the ratio of the sensitivities of the two channels of the analyzer unit.

Accordingly, therefore we get the ellipsometric parameters:

$$\tan^2 \Psi = \frac{(x_1 - b_1 b_2 x_2 + c)}{(b_1 b_2 x_1 - x_2 + c)} \quad (4)$$

$$\cos \Delta = \frac{b_1 x_3 - \sin^2 A \sin^2 P + (b_1 x_4 - \cos^2 A \cos^2 P) \tan^2 \Psi}{\frac{1}{2}(b_1 + 1) \sin 2A \sin 2P \tan \Psi} \quad (5)$$

Here

$$c = b_2(\sin^2 A \sin^2 P - \cos^2 A \cos^2 P) + b_1(x_4 - x_3)$$
$$x_1 = \sin^2 A$$
$$x_2 = \cos^2 A$$

$$x_3 = \cos^2 A \sin^2 P$$
$$x_4 = \sin^2 A \cos^2 P \quad (6)$$

At the same time, in order to calibrate the measuring channel, it is easy to implement a method with finding the azimuths of the analyzer, at equal intensities observed on the photodetectors.

$$\tan A_{1,2} = \tan\Psi \frac{(\sin 2P_2 - a \sin 2P_1)\cos\Delta}{(a\sin^2 P_1 - \sin^2 P_2)} + \tan\Psi \frac{[\cos^2\Delta(\sin 2P_2 - a\sin 2P_1)^2 - 4(a\sin^2 P_1 - \sin^2 P_2)(a\cos^2 P_1 - \cos^2 P_2)]^{1/2}}{2(a\sin^2 P_1 - \sin^2 P_2)} \quad (7)$$

where a is the ratio of the intensities of the switched beams.

When calibrating the measuring path, the spectral dependences of h_a and the difference (A-P) are to be determined. According to expressions (3):

$$I_1 = I_0 h_a \cos^2(A-P)$$
$$I_2 = I_0 \sin^2(A-P)$$
$$I_3 = I_0 h_a \sin^2(A-P)$$
$$I_4 = I_0 \cos^2(A-P) \quad (8)$$
$$h_a^2 = \frac{I_1 I_3}{I_2 I_4}$$
$$\tan^2(P-A) = \left(\frac{I_3 I_2}{I_1 I_4}\right)^{1/2}$$

Calibration of this SE is very simple and is carried out in two stages. At the first stage, the spectrum of the ratio of the channel sensitivities $h_a(\lambda)$, corresponding to the two polarizations after the analyzer and the difference between the angles of the polarizer and the analyzer P-A are measured in the position to the transmission. The formulas given in (8) for four combinations of polarizations for the position in the transmission are simplified:

$$R_1 = \frac{h_a}{tg^2(P-A)};\ R_2 = h_a tg^2(P-A) \quad (9)$$

where R_1, R_2 are the intensity ratios on two photodetectors.

Therefore

$$h_a = (R_1 R_2)^{\frac{1}{2}};\ P - A = arctg\left(\left(\frac{R_2}{R_1}\right)^{\frac{1}{4}}\right) \quad (10)$$

At the second stage, at an angle of incidence of 70° with a silicon sample and a known thin oxide, the ratios of the intensities of the beams R_1, R_2 are measured. By solving the inverse problem, the polarizer angle P, the angle of incidence of radiation on the sample, and the silicon oxide thickness are determined.

1.2. Near-IR 4 mirror achromatic compensator

The proposed compensator should have good transmission characteristics and smooth energy dependence in the range from 260–2000 nm. The restrictions on the total phase shift require in our case $0° < \Delta_r < 90°$ in the entire energy range. In this case, the coaxiality of the incoming and outgoing beams is required.

Based on this, we will design a compensator acting on the principle of phase shift caused by reflection from a metal mirror.

An optimal mirror material must meet the following requirements to function as a good reflective quarter-wave plate:

$$|r_s| = |r_p|;\ \Delta\varphi = |\varphi_s - \varphi_p| = 90° \quad (11)$$

The material must also provide high reflectivity over the entire spectral range, these properties must be nearly constant over a relatively wide range of photon energies and incidence angles to avoid the critical issue of bandwidth and alignment.

Aluminum is a convenient mirror material in the energy range we use. Combined with its high reflectivity, aluminum is a good choice for our purposes.

In addition, it is necessary to find the correct geometry of the phase-shifting device (PD), because the phase difference Δ_r introduced by the compensator depends to a greater extent on the geometry.

Geometric phase analysis showed that a three-mirror PD is capable of rotating the polarization of the incoming beam through the angle $0 < \phi < \pi$. It has been proven that rotation of linear polarization through any angle requires at least four reflections for the final beam path to be collinear with the incoming beam.

Figure 2 shows a diagram of a four-mirror asymmetric PD, which is convenient for implementation.

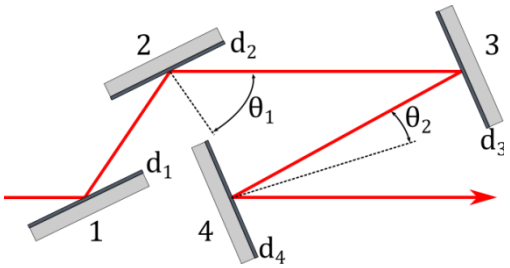

Fig. 2. Optical scheme of a four-mirror asymmetric compensator

The scheme uses four metal mirrors, in pairs (1-2, 3-4), installed at specified angles θ_1 and θ_2 to the incident beam.

The first pair of mirrors are positioned to ensure parallel beam propagation. The second pair of mirrors returns the direction of propagation of radiation to a given axis and are installed in the optical path at a small angle θ_2 to the incident beam to compensate for the sharp increase in Δ with increasing λ.

In this case, the total phase and amplitude displacement is introduced, the values of which can be calculated using the Fresnel reflection coefficients

$$r_p = \frac{n_1\cos\theta_0 - n_0\cos\theta_1}{n_1\cos\theta_0 + n_0\cos\theta_1};\ r_s = \frac{n_0\cos\theta_0 - n_1\cos\theta_t}{n_0\cos\theta_0 - n_1\cos\theta_t} \quad (12)$$

Obviously, these values depend exclusively on the angle of incidence and the refractive indices of air and aluminum.

High-quality aluminum mirrors can be easily manufactured by sputtering Al onto a glass substrate, but it should be borne in mind that in air it is coated with a layer of Al_2O_3 several nanometers thick. This oxide layer slightly changes the optical properties of aluminum-coated mirrors.

Table 1 shows the angles of incidence on the mirrors and the generated phase shifts and amplitude changes.

Table 1. Dependence of the angles of incidence of the beam and the corresponding phase shifts and changes in amplitude

Mirror No	θ (°)	ψ (°)	Δ (°)
1	32.47	44.93	179.18
2	33.20	44.90	179.14
3	33.20	44.92	179.14
4	32.20	44.91	179.12

To verify the obtained models of prototypes of four-mirror achromatic PDs and to confirm the calculated values, experimental studies were carried out in the following configuration.

The polarization properties of the compensator were obtained in the mode of direct measurement on a spectral ellipsometer with SOPS in the range 260–1000 nm; data from literature sources were used to calculate the optical constants.

Figure 3a shows a good correspondence between the experimental and calculated data when determining the thickness of the Al_2O_3 oxide on Al.

Figure 3b shows the curves of the calculated spectral dependences corresponding to the models of a reflective compensator with a set of variable parameters from two angles of installation of the mirrors and four different thicknesses of aluminum oxide on the surface of the mirrors.

For certain sets of parameters, high quality achromatization has been achieved in a wide spectral range. Curve 1 corresponds to the FMC, in which all mirrors have their own oxide 5.5 nm thick. Blocks of parallel mirrors are inclined to the radiation beam at angles of 49° and 41°, respectively. In the short-wavelength region, a sharp change in Δ is observed, leading to an increase in the errors of ellipsometric measurements. Curve 2 corresponds to the case when the radiation beam is incident at an angle $\theta_1 = 49°$ onto a block of mirrors with oxide thicknesses $d_1 = d_2 = 5.5$ nm, and then at an angle $\theta_2 = 41°$ onto a block of mirrors with an oxide $d_3 = 5.5$ nm and $d = 36$ nm. A decline remains in the wavelength range of 200–250 nm. Curve 3 corresponds to a set of parameters:

θ_1 = 49°, θ_2 = 41°, d_1 = 14 nm, d_2 = 21 nm, d_3 = 36 nm, d_4 = 70 nm. Deviations from -90° do not exceed 4° in the spectral range 200–1000 nm. Curve 4 corresponds to a set of parameters: θ_1 = 45°, θ_2 = 52°, d_1 = 36 nm, d_2 = 162 nm, d_3 = 36 nm, d_4 = 76 nm. A fairly flat area is observed in the spectral range of 400–2000 nm.

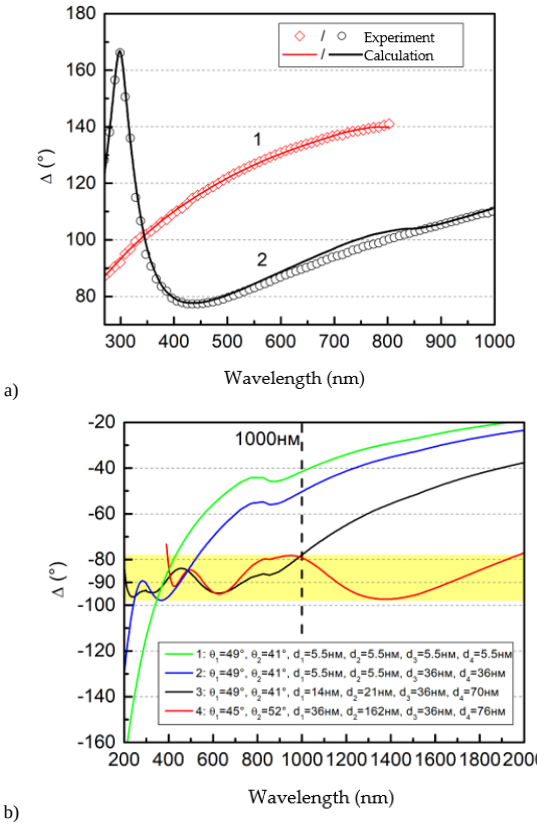

Fig. 3. Spectral dependences of the ellipsometric parameter Δ for: a) layers with a thickness d of Al_2O_3 on Al:1 – d = 5.5 nm; 2 – d = 36 nm, b) a four-mirror asymmetric compensator for different thicknesses d of Al_2O_3 layers on Al and angles of incidence θ_1 and θ_2 of radiation on the mirrors. Curve 1: θ_1 = 49°, θ_2 = 41°, d_1 = 5.5 nm, d_2 = 5.5 nm, d_3 = 5.5 nm, d_4 = 5.5 nm. Curve 2: θ_1 = 49°, θ_2 = 41°, d_1 = 5.5 nm, d_2 = 5.5 nm, d_3 = 36 nm, d_4 = 36 nm. Curve 3: θ_1 = 49°, θ_2 = 41°, d_1 = 14 nm, d_2 = 21 nm, d_3 = 36 nm, d_4 = 70 nm. Curve 4: θ_1 = 45°, θ_2 = 52°, d_1 = 36 nm, d_2 = 162 nm, d_3 = 36 nm, d_4 = 76 nm

1.3. Materials

As objects for experimental studies, confirming the efficiency and high accuracy of the fabricated SE, we used a GaAs/ZnS-quarter-wave device for a CO_2 laser and SiO_2 on Si calibration plates (StepWafer, Ocean Optics).

The standard sample, manufactured by Ocean Optics, is a silicon substrate (Si) coated with a thermal oxide layer (SiO_2). The disc has a diameter of 100 mm and 5 steps of oxide thickness on a calibration plate in the range from 0 to 500 nm. It is ideal for use as a standard sample when measuring the thickness of thin transparent layers on a variety of substrates. Each disc is supplied with a calibration certificate containing information on coordinates (x, y) and their corresponding values (ψ, Δ) and film thickness. The plates are calibrated using a verified ellipsometer and their measurement error, guaranteed by the manufacturer, does not exceed 0.1 nm.

In an experimental study, using the developed SE, the optical properties of $Bi_2Te_{3-x}Se_x$ thin films grown by chemical metalorganic vapor phase epitaxy method (MOVPE) on (0001) Al_2O_3 substrates were studied.

To set the research problem, the measured samples and their production process were fully described. In this case, the samples were examined by alternative methods to confirm the physical characteristics.

The films under study were grown at a temperature of 460°C under conditions of a multiple excess of chalcogenes in the gas phase, had a thickness of ~ 0.5 μm and a mirror surface. The epitaxial nature of the films and their crystal structure of tetradymite are confirmed by X-ray studies. The chemical composition of the films was determined on a Jeol JSM-6480LV scanning electron microscope with a built-in X-MaxN energy dispersive spectrometer.

The optical properties of the samples were investigated by spectral ellipsometry in the range 260–1000 nm. The SE data were compared with the results of electron probe studies, a calibration curve was obtained for the express determination by the SE method of the composition of $Bi_2Te_{3-x}Se_x$ thin films in the concentration range ($0 \le x \le 3$). Multi-angle measurements of the spectra of ellipsometric parameters significantly increase the reliability of measurements in the case of investigations of complex structures with initially unknown optical properties.

2. Results and discussions

2.1. SiO_2 on Si calibration plates

Figure 4 shows the measured and calculated ellipsometric parameters Ψ and Δ for Si/SiO_2 calibration plates with oxide thicknesses of 4 nm and 450 nm. Note that the significant smoothing of the peaks in the infrared region of the spectrum is caused by the imperfection of the rear surface of the plates.

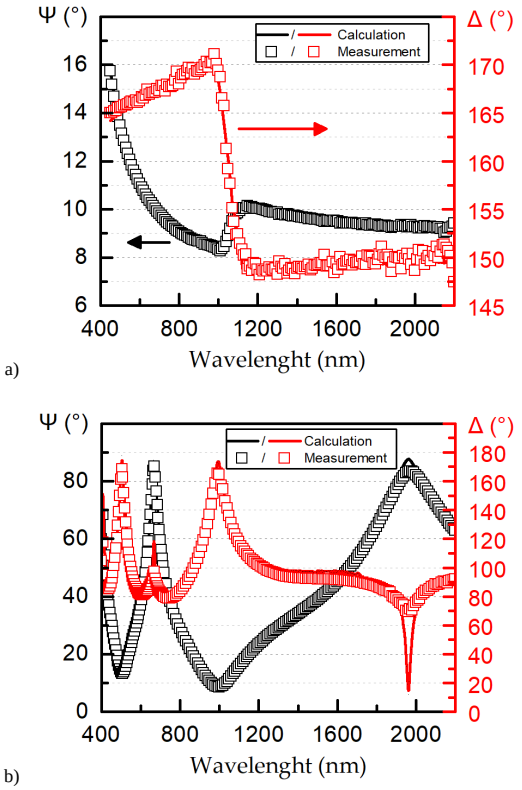

Fig. 4. Spectral dependences of ellipsometric parameters Ψ and Δ for Si/SiO_2: a) SiO_2 thickness 4 nm; b) SiO_2 450 nm thick

Figure 5 shows the dependences of Ψ and Δ on time (noise) for a Si/SiO_2 sample with an oxide thickness of 450 nm at a wavelength of 800 nm and an oxide thickness of 513 nm at a wavelength of 1800 nm. The measurement time for each point was 2 s. The root-mean-square noise at a wavelength of 800 nm and an oxide thickness of 450 nm was 0.0025° (for Ψ) and 0.016° (for Δ); at a wavelength of 1800 nm and an oxide thickness of 513 nm – 0.005° (for Ψ) and 0.03° (for Δ).

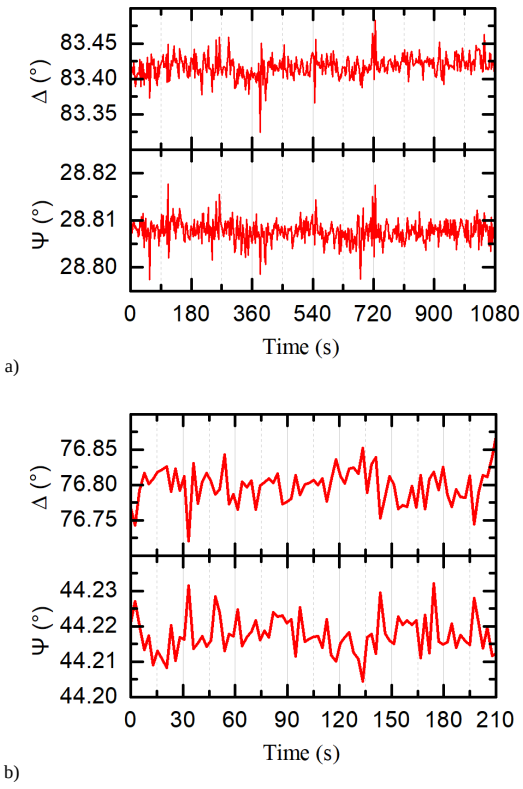

Fig. 5. Time dependences of the parameters Ψ and Δ of the Si/SiO₂ sample: a) with a SiO₂ thickness of 513 nm at a wavelength of 1800 nm; b) with a SiO₂ thickness of 45 nm at a wavelength of 1800 nm. Integration time 2 s

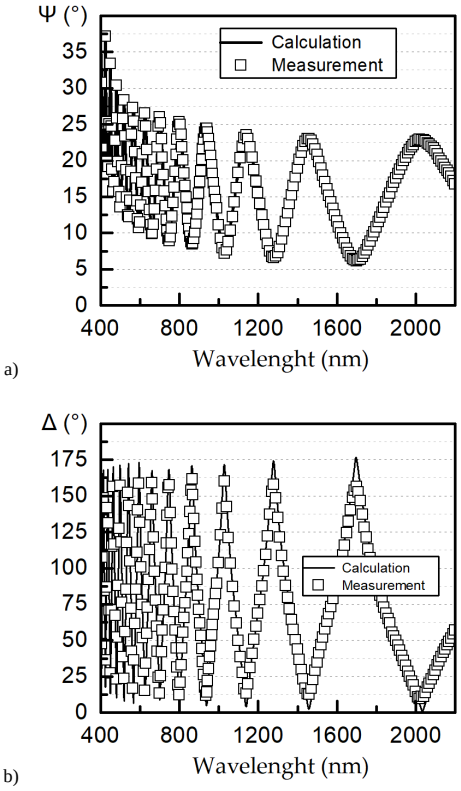

Fig. 6. Spectral dependence of Ψ and Δ for a ZnS film on a GaAs substrate polished on both sides

2.2. GaAs/ZnS structures

To calculate the parameters of the ZnS layer, we used the spectral dependence of the refractive index n according to the simplified Sellmeier formula:

$$n(\lambda)^2 = {n_0}^2 + 1/(1 - \frac{{\lambda_0}^2}{\lambda^2}) \quad (13)$$

where n_0 is the value of the refractive index at an infinite wavelength; λ_0 is the wavelength at which n is equal to infinity. To determine n_0, the calculated parameter n_m was used, which corresponds to the value of the refractive index at a wavelength of λ_m = 550 nm

$${n_m}^2 = {n_0}^2 + 1/(1 - \frac{{\lambda_0}^2}{{\lambda_m}^2}) \quad (14)$$

The spectral dependence of the absorption coefficient k was approximated by an exponential dependence:

$$k(\lambda) = k_m \exp((\lambda_m - \lambda)/\lambda_1) \quad (15)$$

where k_m is the value of the absorption coefficient k at a wavelength of λ_m = 550 nm, λ_1 is the wavelength interval at which k changes by a factor of e.

Figure 6 shows the measured Ψ and Δ spectra for a GaAs/ZnS sample in the 400–2200 nm wavelength range.

Since it is difficult to accurately describe the dispersion in a wide wavelength range with a simplified formula, it was divided into 2 regions: 400–600 nm and 600–2200 nm. In the second range, the ZnS layer thickness d = 1246.6 nm and the parameters n_m = 2.3667, λ_0 = 336 nm, k_m = 0.001, λ_1 = 200 nm were determined by the least squares deviation method. For the same thickness in the first range, the parameters n_m = 2.3579, λ_0 = 297 nm, k_m = 0.001, λ_1 = 200 nm are determined. Figure 7 shows the spectral dependences of the refractive and absorption indices n, k, obtained by the given formulas (13–15) with the indicated coefficients.

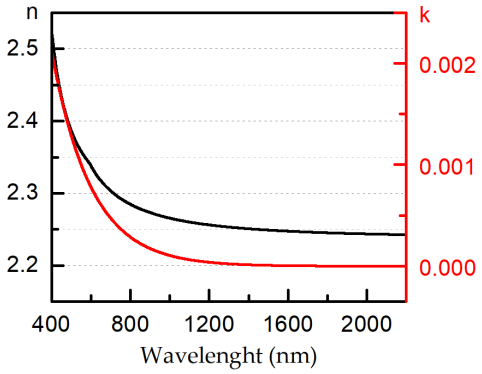

Fig. 7. Spectral dependence of the refractive index n and absorption coefficient k for a ZnS film on a GaAs substrate polished on both sides

2.3. $Bi_2Te_{3-x}Se_x$ topological insulator structures

Figure 8 shows the measured spectral dependence of the ellipsometric angles ψ and Δ of 490 nm thick Bi_2Se_3 and Bi_2Te_3 films deposited on sapphire substrates in the wavelength range 260–1000 nm at incidence angles of 60, 65, and 70°. At these thicknesses, $Bi_2Te_{3-x}Se_x$ films are completely opaque, which makes it possible to use a two-layer (film/surface layer) model to determine its optical properties from the SE spectra.

It was assumed that the surface layer above the films corresponds to the measured ellipsometric spectra. We found that the root-mean-square values of the roughness (rms) of AFM scans over an area of 10 × 10 μm^2 strongly depend on the film thickness. For example, the rms of a 30 nm film was several times higher than that of a 110 nm film. This is due to the transformation of growth modes (3D → 2D) in the process of increasing the film thickness. As a result, upon reaching a thickness of 500 nm, rms was 1–2 nm.

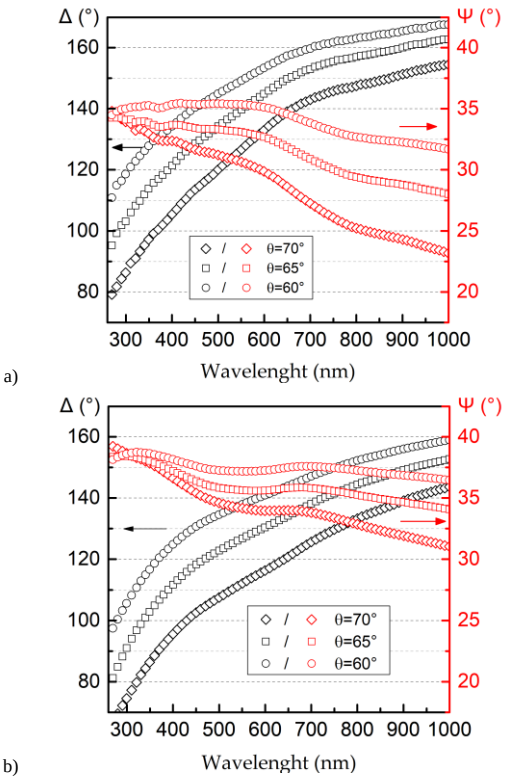

Fig. 8. SE spectra for $Bi_2Te_{3-x}Se_x$ films: a) x = 3; b) x = 0

AFM micrographs and their profiles for such samples show regular triangular terraces 0.95 nm in height, which correspond to a layered structure of the tetradymite type of $Bi_2Te_{3-x}Se_x$ films.

It is assumed that the surface (rough) layer is a mixture of 70% diamond and 30% voids. It was described using the Bruggeman effective medium approximation, which can be successfully used to simulate optical functions of surface roughness and interface layers. Modeling was performed using regression analysis and spectra of the real and imaginary parts of the permittivity were obtained for the entire set of $Bi_2Te_{3-x}Se_x$ films under study (16 samples). To clarify the correlation of some parameters, all spectra were fitted several times using different sets of initial parameters. Each time the fitting procedure gave the same result. The simulation results for five $Bi_2Te_{3-x}Se_x$ films with different x are shown in figure 9.

The strongest changes in the spectra of optical parameters of $Bi_2Te_{3-x}Se_x$ films depend on their composition x. Changes in the parameters are observed in the red and near-IR regions of the spectrum, and the short-wavelength part of the spectra is weakly sensitive to the composition of the films.

Figure 10 shows how the spectral position of the maximum of the imaginary ($\varepsilon 2$) parts of the dielectric function depends on their chemical composition of the studied $Bi_2Te_{3-x}Se_x$ films. It should be noted that this position is observed in the long-wavelength part of the spectra.

In a wide range of concentrations x, a monotonic change in the position of the maximum is observed depending on the composition of the films, which makes it possible to use the SE data to determine the composition of $Bi_2Te_{3-x}Se_x$ films. The value of the real ($\varepsilon 1$) parts of the dielectric function in the 800–900 nm range is also suitable for a quick assessment of the composition of $Bi_2Te_{3-x}Se_x$ films using SE measurements (figure 9a).

Published data on the Bi_2Te_3-Bi_2Se_3 system are contradictory. For example, some authors state that the $Bi_2Te_{3-x}Se_x$ compounds can be considered as a limited solid solution system with the Bi_2Te_2Se compound below the solidus line (500°C). Our XRD and SE data on monotonic changes in the lattice parameters and optical properties of $Bi_2Te_{3-x}Se_x$ films, depending on their composition, are consistent with the concept of the formation of a continuous series of solid solutions due to the gradual complete filling of selenium atoms into the inner rows in five-layer Te-Bi-Se blocks. (Te)-Bi-Te.

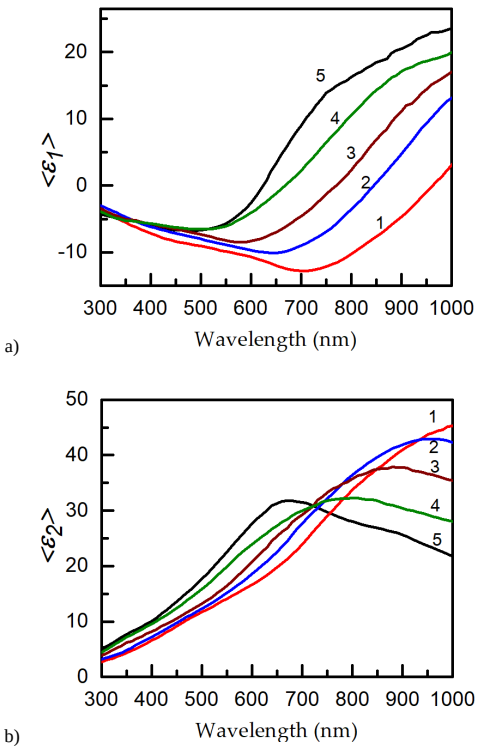

Fig. 9. Spectral dependence of the real ε_1 (a) and imaginary ε_2 (b) parts of the dielectric function for five $Bi_2Te_{3-x}Se_x$ films with x = 0, 0.25, 0.48, 1.5, 3.0 (curves 1 ÷ 5, respectively)

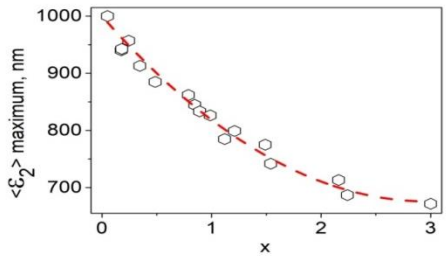

Fig. 10. Correlation between the position of the maxima in the ε_2 spectra of the $Bi_2Te_{3-x}Se_x$ researched films and their chemical composition

The good crystal structure and high quality of the surface of the films with a thickness of about 500 nm are confirmed by X-ray diffraction and atomic force microscopy. It is shown that multi-angle SE is a powerful method for studying the optical properties of $Bi_2Te_{3-x}Se_x$ films. There is no expected inflection in the dependence of the optical properties of the researched films on the composition, especially near x = 1, at which selenium atoms completely occupy the inner rows in the five-layer Te-Bi-Se (Te)-Bi -blocks.

The study shows the possibility of joint use of the proposed ellipsometric setup in the system with other analytical methods and means for monitoring the optical and physical properties when obtaining structures based on $Bi_2Te_{3-x}Se_x$. There are ample opportunities for studying the topological properties and applications of devices based on these compositions.

2.4. Compensator

The phase shift spectra of the FMC, in which two mirrors have an oxide 5.5 nm thick and two mirrors are 36 nm thick are shown in Figure 11. It should be noted that the phase shift deviations of the FMC, from 90° significantly decrease in the measured spectral range from 270 to 800 nm compared with the calculated spectral dependence of the phase shift for the case when all mirrors have only their own oxide.

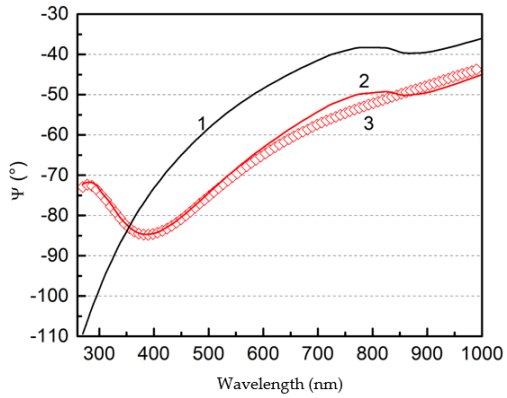

Fig. 11. Spectral dependences of the phase shift of a four-mirror asymmetric compensator with incidence angles of 51° and 30°: 1 – Calculation for the case when 4 mirrors have their own oxide 5.5 nm thick. 2 – two mirrors with their own oxide (51°) and two with an oxide thickness of 36 nm (30°), 3 – measured values

Figure 12 illustrates the possibilities of accurate and unambiguous determination of the spectra of the ellipsometric parameter Δ of the reference sample of thick SiO_2 oxide on Si in the automatic mode of sequential measurements with and without a FMC at each wavelength.

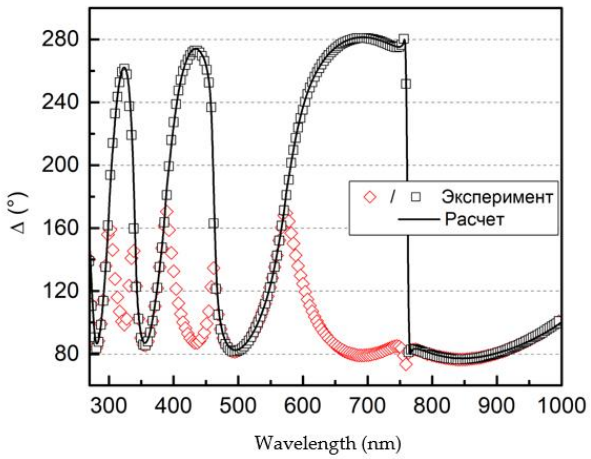

Fig. 12. Spectra of the ellipsometric parameter Δ of the reference sample of SiO_2 oxide with a thickness of 513 nm on Si: 1 – measurements with a compensator; 2 – measurements without compensator (oints – measurements, line – calculation)

The time dependences of the phase shift Δ FMC shown in figure 13, measured at wavelengths of 288 nm and 550 nm, confirm high reproducibility (up to 0.001°) and long-term stability of the compensator under standard laboratory conditions. When measuring the compensator as a sample, Δ is determined in the range of 0–180°.

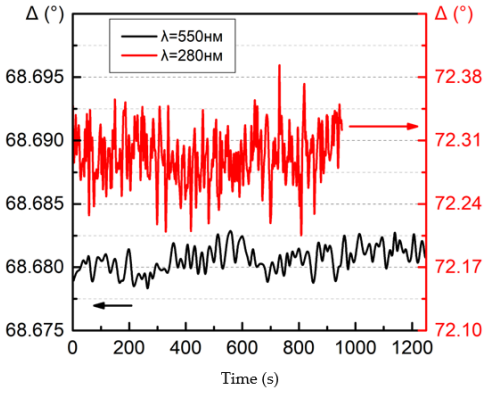

Fig. 13. Time dependences of the phase shift of the. FMC

The results of measurements and calculations confirm the possibility of creating achromatic four-mirror compensators in the spectral range of 200–2000 nm, which is widely used by modern spectral ellipsometers.

The time dependences of the phase shift Δ of the FMC, measured at wavelengths of 288 nm and 550 nm, confirm the high reproducibility and stability of measurements on the LED ellipsometer and the stability of the compensator itself under standard laboratory conditions.

It is planned to manufacture a compensator for the spectral range of 260–1000 nm, the calculated characteristics of which correspond to curve 3 in Figure 3b. It should be noted the low cost of the proposed FMC, the high ratio of the aperture to the length of the compensator, the possibility of precise adjustment of the angles of inclination of the mirrors using a goniometer and autocollimator, as well as the elimination of the need for thermostating of the compensator.

It has been shown experimentally that the use of the proposed simple design of the SE based on the MDR-41 monochromator makes it possible to achieve high technical characteristics. Optimization of the illumination scheme of the entrance slit of the monochromator and the use of GT prisms with a larger aperture will significantly improve the technical characteristics. The described approach provides ample opportunities for creating precision SE with an extended spectral range. Thus, the implementation of a solar cell with an operating wavelength range of 400–5000 nm is possible with a device for aligning orthogonally polarized beams made of YVO4. In this case, it is optimal to use pulsed radiation sources and photodetectors developed for the spectral range of 2–5 microns.

The described ellipsometer using as emitters sets of pairs of identical intense LEDs located, for example, on a disk with a horizontal axis of rotation, does not require interruption of the beams behind the exit slit of the monochromator and provides high-speed ellipsometric measurements at selected wavelengths in the spectral range of 260–1700 nm. The speed of measurements at the wavelengths of LED radiation is completely determined by the time characteristics of switching on and off and their intensity.

The features of the dispersion dependences of the promising material α-BBO do not allow the fabrication of GT prisms with an operating range of 200–3500 nm. We have developed an achromatic device for converging two beams based on a Wollaston prism, at the output of which the combination of orthogonally polarized beams in this spectral range is implemented. Based on this device, it is planned to manufacture a SE with an operating range of 200–3500 nm. Devices for converging orthogonally polarized beams and their separation on the basis of doped silicon wafers installed at the Brewster angle and ZnSe (ZnS) dividing wafers extend the spectral range of SE to 12–18 μm.

3. Conclusions

The new approach developed in the article significantly expands the measuring capabilities of sensitive ellipsometers with switching orthogonal polarization states. The elimination of low-frequency polarization modulators reduces the loss of beam intensity, simplifies the design of the SE, and makes it possible to significantly increase the rate of ellipsometric measurements using high-speed pulsed radiation sources. At the selected wavelengths, it is possible to determine the spatial distribution of ellipsometric parameters over the area of the studied plates, quickly measure the change in the parameters of liquid and gaseous flows in time, and kinetic measurements in the pump/probe configuration. SE can be used to control growth processes. This research shows the possibility of joint use of the proposed ellipsometric setup in the system with other analytical methods and means for monitoring the optical and physical properties when obtaining structures based on $Bi_2Te_{3-x}Se_x$.

References

[1] Acher O., Bigan E., Drévillon B.: Improvements of phase-modulated ellipsometry. Rev. Sci. Instrum. 60, 1989 [http://doi.org/10.1063/1.1140580].

[2] Alonso M. I., Garriga M.: Optical properties of semiconductors. Springer International Publishing Vol. 212, 2018.

[3] Aspnes D. E.: Spectroscopic ellipsometry — Past, present, and future. Thin Solid Films 571, 2014, 334–344 [http://doi.org/10.1016/j.tsf.2014.03.056].

[4] Azzam R. M. A.: Photopolarimetric measurement of the Mueller matrix by Fourier analysis of a single detected signal. Opt. Lett. 2, 1978, [http://doi.org/10.1364/ol.2.000148].

[5] Collins R. W., Koh J.: Dual rotating-compensator multichannel ellipsometer: instrument design for real-time Mueller matrix spectroscopy of surfaces and films. Journal of the Optical Society of America A 16, 1999, 1997 [http://doi.org/10.1364/JOSAA.16.001997].

[6] Fujiwara H.: Spectroscopic Ellipsometry: Principles and Applications. John Wiley and Sons, 2007.

[7] Furchner A., Walder C., Zellmeier M., Rappich J., Hinrichs K.: Broadband infrared Mueller-matrix ellipsometry for studies of structured surfaces and thin films. Appl. Opt. 57, 2018, 7895 [http://doi.org/10.1364/AO.57.007895].

[8] Garcia-Caurel E., de Martino A., Drévillon B.: Spectroscopic Mueller polarimeter based on liquid crystal devices. Thin Solid Films 455–456, 2004, 120–123 [http://doi.org/10.1016/j.tsf.2003.12.056].

[9] Garcia-Caurel E., de Martino A., Gaston J.-P., Yan L.: Application of Spectroscopic Ellipsometry and Mueller Ellipsometry to Optical Characterization. Applied Spectroscopy 67, 2013, 1–21 [http://doi.org/10.1366/12-06883].

[10] Hinrichs K., Eichhorn K. J., Ertl G., Mills D. L., Lüth H.: Ellipsometry of Functional Organic Surfaces and Films. Springer Series in Surface Sciences Vol. 52, Berlin, Heidelberg, 2014.

[11] Kovalev V. I., Rukovishnikov A. I., Kovalev S. V., Kovalev V. V., Rossukanyi N. M.: An achromatic four-mirror compensator for spectral ellipsometers. Opt. Spectrosc. 123, 2017 [http://doi.org/10.1134/S0030400X1707013X].

[12] Kovalev V. I., Rukovishnikov A. I., Kovalev S. V., Kovalev V. V.: An LED multichannel spectral ellipsometer with binary modulation of the polarization state. Instruments and Experimental Techniques 57, 2014 [http://doi.org/10.1134/S002044121405008X].

[13] Kovalev V. I., Rukovishnikov A. I., Kovalev S. V., Kovalev V. V.: LED broadband spectral ellipsometer with switching of orthogonal polarization states. J. Opt. Technol. 2016, 83, 181 [http://doi.org/10.1364/JOT.83.000181.

[14] Kovalev V. V., Kuznetsov P. I., Yakushcheva G. G., Yapaskurt O. V., Kovalev V. I., Rukovishnikov A. I., Kovalev S. V.: MOVPE deposition and optical properties of thin films of a Bi2Te3-xSex topological insulator. J. Phys. Conf. Ser. 1199, 2019, 012038 [http://doi.org/10.1088/1742-6596/1199/1/012038].

[15] Kovalev, V.I., Rukovishnikov, A.I., Rossukanyi, N.M., Kovalev, S. V., Kovalev, V. V., Amelichev, V. V., Kostyuk, D. V., Vasil'ev, D. V., Orlov, E. P. LED magneto-optical ellipsometer with the switching of orthogonal polarization states. Instruments and Experimental Techniques 59, 2016, 707–711 [http://doi.org/10.1134/S0020441216040084].

[16] Kroning A., Furchner A., Aulich D., Bittrich E., Rauch S., Uhlmann P., Eichhorn K. J., Seeber M., Luzinov I., Kilbey S. M., et al.: In Situ Infrared Ellipsometry for Protein Adsorption Studies on Ultrathin Smart Polymer Brushes in Aqueous Environment. ACS Appl. Mater. Interfaces 7, 2015, 12430–12439 [http://doi.org/10.1021/am5075997].

[17] Li K., Wang S., Wang L., Yu H., Jing N., Xue R., Wang Z.: Fast and Sensitive Ellipsometry-Based Biosensing. Sensors 18, 2017, 15 [http://doi.org/10.3390/s18010015].

[18] Losurdo M., Bergmair M., Bruno G., Cattelan D., Cobet C., de Martino A., Fleischer K., Dohcevic-Mitrovic Z., Esser N., Galliet M., et al.: Spectroscopic ellipsometry and polarimetry for materials and systems analysis at the nanometer scale: State-of-the-art, potential, and perspectives. J. Nanoparticle 11, 2009, 1521–1554 [http://doi.org/10.1007/s11051-009-9662-6].

[19] de Martino A., Kim Y.-K., Garcia-Caurel E., Laude B., Drévillon B.: Optimized Mueller polarimeter with liquid crystals. Opt. Lett. 28, 2003, 616 [http://doi.org/10.1364/OL.28.000616].

[20] Schmidtling T., Pohl U. W., Richter W., Peters S.: In situ spectroscopic ellipsometry study of GaN nucleation layer growth and annealing on sapphire in metal-organic vapor-phase epitaxy. J. Appl. Phys. 98, 2005, [http://doi.org/10.1063/1.1999033].

[21] Tompkins H. G., Irene E. A.: Handbook of Ellipsometry. William Andrew Publishing, 2005.

[22] Yim C., O'Brien M., McEvoy N., Winters S., Mirza I., Lunney J. G., Duesberg G. S.: Investigation of the optical properties of MoS2 thin films using spectroscopic ellipsometry. Applied Physics Letters 104, 2014 [http://doi.org/10.1063/1.4868108].

Ph.D. Vladimir Kovalev
e-mail: vladimirkovalev.inc@gmail.com

Scientific researcher – Institute of Radio-Engineering and Electronics of Russian Academy of Sciences. Modern solutions of spectral ellipsometry, the development of new polarization elements and devices.

http://orcid.org/0000-0003-3570-393X

Prof. Saygid Uvaysov
e-mail: uvaysov@yandex.ru

Head of the Radio-Electronic Means Design and Production Department of the Radio Engineering and Telecommunications Systems Institute, MIREA – Russian Technological University.
Scopus Author ID: 55931417100
Researcher ID: H-6746-2015

http://orcid.org/0000-0003-1943-6819

Ph.D. Marcin Bogucki
e-mail: m.bogucki@pollub.pl

Assistant professor on Department of Automation, Faculty of Mechanical Engineering, Lublin University of Technology, Poland.

Research interests: design of experiments, empirical model building, automation, robotics;

http://orcid.org/0000-0001-5296-3827

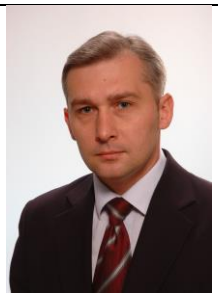

otrzymano/received: 20.11.2021 *przyjęto do druku/accepted: 15.12.2021*